Diagnosing selenium plasmas using Se XXVI and Se XXV line cluster ratios

Arati Dasgupta and K. G. Whitney
Radiation Hydrodynamics Branch, Plasma Physics Division, Naval Research Laboratory, Washington, DC 20375

Hong Lin Zhang
Department of Astronomy, Ohio State University, Columbus, Ohio 43210

D. H. Sampson
Department of Astronomy and Astrophysics, The Pennsylvania State University, University Park, Pennsylvania 16802
(Received 24 July 1996)

Ratios of resonance and satellite line clusters in fluorinelike (Se XXVI) and neonlike (Se XXV) ions are used in the development of a diagnostics procedure for analyzing high density, optically thin selenium plasmas. The atomic model employed in this work to calculate line intensities for $n=2$–3 transitions includes detailed fine-structure levels for the $n=3$ excited configurations, $n=3$ inner-shell excited states at the configuration level, and lumped $n=4$ levels for both Se XXVI and Se XXV. All relevant atomic processes connecting these levels and all collisional couplings among the excited states are included in the model. The collisional and radiative data such as collisional excitation and ionization (including inner shell), and both radiative and dielectronic recombination rates, are obtained using several different sophisticated atomic codes. From these data, collisional-radiative equilibrium solutions to a fully coupled single set of rate equations are obtained for the populations of the ground as well as all excited levels, and used for the computation of the line intensities. For calculations of the satellite line intensities, populations of the doubly excited states are obtained from the sum of contributions from dielectronic recombination of ground states and inner-shell excitation of singly excited states. Because experimental L-shell spectra of the $n=2$–3 resonance and satellite lines contain many lines, often they are not spectroscopically resolved unless obtained under extremely high resolution. Therefore, instead of using individual lines which often cannot be separated experimentally from other overlapping lines, resonance line as well as satellite line configuration clusters in Se XXVI and Se XXV are used in this diagnostic work. The intensity ratios of the resonance and satellite line clusters are functions of both electron temperature and ion density and simultaneous determinations of these quantities are possible using contour plots of specific cluster ratios. These plots are obtained for a wide range of densities and temperatures, and they reflect the detailed effects of the different atomic processes on the intensities of the resonance and satellite lines as a function of plasma conditions. [S1063-651X(97)12903-8]

PACS number(s): 52.70.−m, 32.30.−r, 34.10.+x

I. INTRODUCTION

X-ray emission spectra from the K shell of low atomic number (Z) elements provide valuable information with which to assess plasma conditions and x-ray emission performance in a variety of laboratory plasmas [1–4]. These soft x-ray lines are also used to diagnose K ions for astrophysical plasmas [5–8]. Some of these ions also exist as impurities in tokamak discharges [9,10]. In all of these plasmas, ratios involving H- and He-like lines have been useful in obtaining diagnostics of low-Z ions [11,12].

A procedure is described by Coulter, Whitney, and Thornhill [2], and further evaluated by Apruzese *et al.* [13] for self-consistently inferring both temperatures and densities from K-shell line ratio and power output data from z-pinch plasmas. A unique determination of both these quantities is possible if one requires that the calculated power output from K-shell emissions as well as the calculated ratio of hydrogenlike Lyman-α to heliumlike $n=2$ to $n=1$ emissions be simultaneously in agreement with measured values of these same quantities. To carry out this comparison, one needs to calculate a set of contours as a function of electron temperature and ion density of both the power output from the K shell and the ratio of hydrogenlike to heliumlike line emissions. The calculations are done with a minimum of assumptions about the spatial structure or temporal history of the z-pinch plasma. Thus a uniform plasma is assumed, which has the size of a measured K-shell emission region, and the plasma is assumed to be in *collisional-radiative equilibrium* (CRE). Because a given-sized cylindrical plasma is assumed, the equilibrium calculations for this procedure self-consistently include the effects of photoexcitations, deexcitations, and ionizations.

The generalization of this K-shell diagnostic procedure to the L shell has two difficulties. First, in analogy to the K-shell analysis, one needs to substitute the Ne-like for the He-like closed-shell system, and to compare emissions from this ion with those from the neighboring F-like ion. In the case of the K shell, it is generally easy to filter out radiation below the K-series lines in order to measure the He-like plus H-like power output since there are no strong emissions from ionization states above the K shell. However, to isolate the power output from Ne- and F-like emissions, one must also filter out, in general, higher-lying line emissions from the O-like, N-like, etc. ionization stages. Thus the procedures that are used in Refs. [2] and [13] need to be extended by

providing a set of contours other than power output with which to complement the F-to-Ne line ratio contours. Second, lines in the K-series spectrum are generally well isolated and ratios of individual lines are often measured. In the L shell, configuration states have more complex multiplet structures than those in the K shell, and line emissions from these states are less isolated, often overlapping, and more difficult to model [14]. Comparisons of calculated and experimental emission ratios may more often be made, in this case, using line clusters rather than individual lines.

The x-ray spectra of L-shell ions are also rich in structure due to the large number of overlapping satellite lines that accompany the resonance lines. Identification of these lines for diagnostic calculations poses challenges that are only recently being addressed [14–18]. However, diagnostic research involving L-shell ions, while not as extensive as that involving K-shell ions, provides potentially more rewards.

The intensity ratios of F- and Ne-like lines are sensitive to electron temperature, density, and rates of ionization, and different line ratios need to be used to infer these different plasma parameters. The density of a plasma is usually inferred from the intensity ratios of two lines of the same ion when the upper levels for both of the lines are collisionally excited, but only one of them has a strong radiative decay, while the other is depopulated by electron collisions. This situation is more prevalent in the L shell than the K shell. Different excitation mechanisms and multiplet structures of lines imply different dependences on the plasma parameters [19,20]. The intensity ratios of two allowed lines of the same ion generally cannot be used to infer the plasma temperature. Ratios of resonance to dielectronic satellite lines, however, provide a very good temperature diagnostic tool, since the upper levels of these lines are populated mainly from the same ground state: for resonance lines, by direct collisional excitation, whereas for satellite lines, mainly by dielectronic recombination (DR). Intensity ratios of two resonance lines from neighboring ions are also good for inferring temperatures or the rate of temperature change, and, therefore, the state of ionization of the plasma. Thus the ratio of two collisionally excited lines or line clusters from neighboring ion stages can generate a temperature-dependent expression for the relative ion fractions. However, the intensity ratios of the resonance lines of two neighboring ions is also density sensitive.

Most diagnostics work utilizes these dependences of different lines on different plasma conditions to separately determine the temperature or the density of the plasma. However, even though some line ratios are more temperature sensitive while others are more density sensitive, the intensity ratios of most lines are more often dependent on both electron temperature T_e and ion density n_i [14]. Thus more reliable determinations of these quantities require analyses of the simultaneous dependences of the line ratios on T_e and n_i, as was done in Refs. [2] and [13]. In this present work, we will investigate these dependences by presenting the line ratios as isocontours in temperature and density space. Overlaps of mostly density sensitive contours with mostly temperature dependent contours can then be used to determine the electron temperature and the ion density simultaneously.

In Sec. II, the atomic model on which this work is based is described. It is an extension of a previously developed

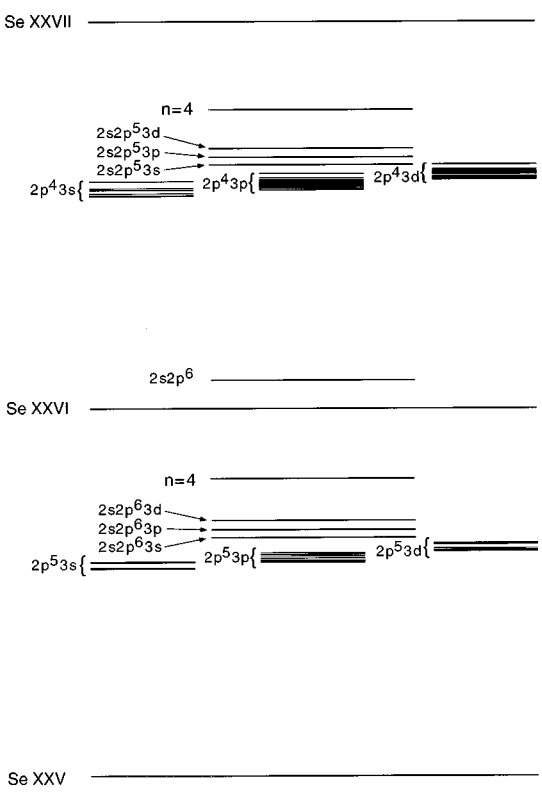

FIG. 1. Energy-level diagram for Se XXVI and Se XXV as used in our atomic model. The model includes 26 (4 $2p^5 3s$, 10 $2p^5 3p$, and 12 $2p^5 3d$) and 57 (8 $2p^4 3s$, 21 $2p^4 3p$, and 28 $2p^4 3d$) multiplet levels for the $n=3$ excited states for Se XXV and Se XXVI, respectively.

model of Dasgupta *et al.* [21]. This extension utilizes fully relativistic atomic data that was calculated using codes developed primarily by two of the authors [22–28], and also the codes of Refs. [29–32]. This data is incorporated into a full set of rate equations from which ion populations are calculated in the CRE approximation under the assumption of an optically thin plasma. From these populations, contours describing resonance line emission behavior are computed. These results are presented in Sec. III. In general, analyses of L-shell spectra must take into account contributions of satellite line emissions that adjoin or overlap with the resonance lines. The effects of satellite lines on line cluster contour plots are discussed in Sec. IV.

II. ATOMIC MODEL

The energy level diagram of the model that we used for analyzing $n=3$ line emission from the fluorinelike (Se XXVI) and neonlike (Se XXV) ionization stages is shown in Fig. 1. This atomic structure is embedded in a configuration state model of the remainder of the selenium ionization stages [33]. The combined model contains the atomic model for Se XXV that is described in Ref. [21] and a similar, but larger, atomic model for Se XXVI, which is listed in Table I. Note that the two multiplet levels of the $2s^2 2p^5$ ground state of Se XXVI are shown as two separate levels in Table I and all the energies and radiative decay rates shown are with respect to the lower lying $J=\frac{3}{2}$ level, although in solving the rate equations we ignore the splittings of this $2s^2 2p^5$ state and

TABLE I. Level identifications, jj- and LS-coupling labels, total angular momentum J, energies and radiative decay rates to the ground level $2s^22p^5$ ($J=\frac{3}{2}$) for Se XXVI. Notation $a[b]$ means $a\times10^b$.

Level	LS state	jj state	J	Energy (eV)	A^r (s^{-1})
1	$2s^22p^5\ ^2P^o$	$[2s^2p_{1/2}^2 2p_{3/2}^3]_{3/2}$	$\frac{3}{2}$	0.0	
2	$2s^22^5\ ^2P^o$	$[2s^2p_{1/2}2p_{3/2}^4]_{1/2}$	$\frac{1}{2}$	4.27[2]	
3	$2s2^6\ ^2S$	$[2s2p_{1/2}^2 2p_{3/2}^4]_{1/2}$	$\frac{1}{2}$	2.138[2]	2.004[11]
4	$2s^2p^4(^3P)3s\ ^4P$	$[2s^22p_{1/2}^2 2p_{3/2}^2]_2 3s$	$\frac{5}{2}$	1.4992[3]	5.860[11]
5	$2s^22p^4(^3P)3s\ ^2P$	$[2s^22p_{1/2}^2 2p_{3/2}^2]_2 3s$	$\frac{3}{2}$	1.5040[3]	6.019[12]
6	$2s^22p^4(^1S)3s\ ^2S$	$[2s^22p_{1/2}^2 2p_{3/2}^2]_0 3s$	$\frac{1}{2}$	1.5184[3]	2.543[12]
7	$2s^22p^4(^3P)3s\ ^4P$	$[2s^22p_{1/2}2p_{3/2}^3]_1 3s$	$\frac{3}{2}$	1.5400[3]	1.635[12]
8	$2s^22p^4(^3P)3s\ ^2P$	$[2s^22p_{1/2}2p_{3/2}^3]_1 3s$	$\frac{1}{2}$	1.5438[3]	2.606[12]
9	$2s^22p^4(^3P)3p\ ^4P^o$	$[2s^22p_{1/2}2p_{3/2}^2]_2 3p_{1/2}$	$\frac{3}{2}$	1.5441[3]	
10	$2s^22p^4(^3P)3p\ ^4D^o$	$[2s^22p_{1/2}^2 2p_{3/2}^2]_2 3p_{1/2}$	$\frac{5}{2}$	1.5459[3]	
11	$2s^22p^4(^1D)3s\ ^2D$	$[2s^22_{1/2}2p_{3/2}^3]_2 3s$	$\frac{5}{2}$	1.5528[3]	3.113[12]
12	$2s^22p^4(^1D)3s\ ^2D$	$[2s^22p_{1/2}2p_{3/2}^3]_2 3s$	$\frac{3}{2}$	1.5542[3]	4.176[11]
13	$2s^22p^4(^3P)3p\ ^2P^o$	$[2s^22p_{1/2}^2 2p_{3/2}^2]_2 3p_{3/2}$	$\frac{1}{2}$	1.5547[3]	
14	$2s^22p^4(^3P)3p\ ^2D^o$	$[2s^22p_{1/2}^2 2p_{3/2}^2]_2 3p_{3/2}$	$\frac{5}{2}$	1.5556[3]	
15	$2s^22p^4(^3P)3p\ ^4D^o$	$[2s^22p_{1/2}^2 2p_{3/2}^2]_2 3p_{3/2}$	$\frac{7}{2}$	1.5564[3]	
16	$2s^22p^4(^1S)3p\ ^2P^o$	$[2s^22p_{1/2}^2 2p_{3/2}^2]_0 3p_{1/2}$	$\frac{1}{2}$	1.5649[3]	
17	$2s^22p^4(^3P)3p\ ^4S^o$	$[2s^22p_{1/2}^2 2p_{3/2}^2]_2 3p_{3/2}$	$\frac{3}{2}$	1.5708[3]	
18	$2s^22p^4(^3P)3p\ ^4D^o$	$[2s^22p_{1/2}^2 2p_{3/2}^2]_0 3p_{3/2}$	$\frac{3}{2}$	1.5762[3]	
19	$2s^22p^4(^3P)3p\ ^4P^o$	$[2s^22p_{1/2}2p_{3/2}^3]_1 3p_{1/2}$	$\frac{1}{2}$	1.5835[3]	
20	$2s^22p^4(^3P)3p\ ^2P^o$	$[2s^22p_{1/2}2p_{3/2}^3]_1 3p_{1/2}$	$\frac{3}{2}$	1.5865[3]	
21	$2s^22p^4(^3P)3p\ ^4P^o$	$[2s^22p_{1/2}2p_{3/2}^3]_1 3p_{3/2}$	$\frac{5}{2}$	1.5956[3]	
22	$2s^22p^4(^1D)3p\ ^2F^o$	$[2s^22p_{1/2}2p_{3/2}^3]_2 3p_{1/2}$	$\frac{5}{2}$	1.5979[3]	
23	$2s^22p^4(^3P)3p\ ^2S^o$	$[2s^22p_{1/2}2p_{3/2}^3]_1 3p_{3/2}$	$\frac{1}{2}$	1.5987[3]	
24	$2s^22p^4(^3P)3p\ ^2D^o$	$[2s^22p_{1/2}2p_{3/2}^3]_1 3p_{3/2}$	$\frac{3}{2}$	1.599[3]	
25	$2s^22p^4(^3P)3s\ ^4P$	$[2s^22p_{3/2}^4]_0 3s$	$\frac{1}{2}$	1.6014[3]	2.357[12]
26	$2s^22p^4(^1D)3p\ ^2F^o$	$[2s^22p_{1/2}2p_{3/2}^3]_2 3p_{3/2}$	$\frac{7}{2}$	1.6082[3]	
27	$2s^22p^4(^1D)3p\ ^2P^o$	$[2s^22p_{1/2}2p_{3/2}^3]_2 3p_{3/2}$	$\frac{3}{2}$	1.6090[3]	
28	$2s^22p^4(^3P)3d\ ^4D$	$[2s^22p_{1/2}^2 2p_{3/2}^2]_2 3d_{3/2}$	$\frac{5}{2}$	1.6114[3]	8.192[09]
29	$2s^22p^4(^3P)3d\ ^4D$	$[2s^22p_{1/2}^2 2p_{3/2}^2]_2 3d_{3/2}$	$\frac{3}{2}$	1.6117[3]	1.426[11]
30	$2s^22p^4(^3P)3d\ ^4D$	$[2s^22p_{1/2}^2 2p_{3/2}^2]_2 3d_{5/2}$	$\frac{7}{2}$	1.6124[3]	
31	$2s^22p^4(^1D)3p\ ^2D^o$	$[2s^22p_{1/2}2p_{3/2}^3]_2 3p_{3/2}$	$\frac{5}{2}$	1.6126[3]	
32	$2s^22p^4(^3P)3d\ ^4P$	$[2s^22p_{1/2}^2 2p_{3/2}^2]_2 3d_{3/2}$	$\frac{1}{2}$	1.6134[3]	4.439[11]
33	$2s^22p^4(^1D)3p\ ^2D^o$	$[2s^22p_{1/2}2p_{3/2}^3]_2 3p_{1/2}$	$\frac{3}{2}$	1.6147[3]	
34	$2s^22p^4(^3P)3d\ ^4F$	$[2s^22p_{1/2}^2 2p_{3/2}^2]_2 3d_{5/2}$	$\frac{9}{2}$	1.6158[3]	
35	$2s^22p^4(^3P)3d\ ^2F$	$[2s^22p_{1/2}^2 2p_{3/2}^2]_2 3d_{3/2}$	$\frac{7}{2}$	1.6167[3]	
36	$2s^22p^4(^3P)3d\ ^2P$	$[2s^22p_{1/2}^2 2p_{3/2}^2]_2 3d_{5/2}$	$\frac{1}{2}$	1.6212[3]	1.914[13]
37	$2s^22p^4(^3P)3d\ ^4P$	$[2s^22p_{1/2}^2 2p_{3/2}^2]_2 3d_{5/2}$	$\frac{3}{2}$	1.6251[3]	1.989[13]
38	$2s^22p^4(^1D)3p\ ^2P^o$	$[2s^22p_{1/2}2p_{3/2}^3]_2 3p_{3/2}$	$\frac{1}{2}$	1.6273[3]	
39	$2s^22p^4(^3P)3d\ ^2D$	$[2s^22p_{1/2}^2 2p_{3/2}^2]_2 3d_{5/2}$	$\frac{5}{2}$	1.6284[3]	2.815[13]
40	$2s^22p^4(^3P)3d\ ^4F$	$[2s^22p_{1/2}^2 2p_{3/2}^2]_0 3d_{3/2}$	$\frac{3}{2}$	1.6343[3]	1.511[13]
41	$2s^22p^4(^1S)3d\ ^2D$	$[2s^22p_{1/2}^2 2p_{3/2}^2]_0 3d_{5/2}$	$\frac{5}{2}$	1.6369[3]	1.845[13]
42	$2s^22p^4(^3P)3d\ ^4D$	$[2s^22p_{1/2}2p_{3/2}^3]_1 3d_{3/2}$	$\frac{1}{2}$	1.6499[3]	1.419[11]
43	$2s^22p^4(^3P)3d\ ^2P$	$[2s^22p_{1/2}2p_{3/2}^3]_1 3d_{3/2}$	$\frac{3}{2}$	1.6539[3]	1.379[12]
44	$2s^22p^4(^3P)3d\ ^4F$	$[2s^22p_{1/2}2p_{3/2}^3]_1 3d_{5/2}$	$\frac{7}{2}$	1.6547[3]	
45	$2s^22p^4(^3P)3p\ ^4D^o$	$[2s^22p_{3/2}^4]_0 3p_{1/2}$	$\frac{1}{2}$	1.6560[3]	
46	$2s^22p^4(^1S)3p\ ^2P^o$	$[2s^22p_{3/2}^4]_0 3p_{3/2}$	$\frac{3}{2}$	1.6577[3]	
47	$2s^22p^4(^3P)3d\ ^4F$	$[2s^22p_{1/2}2p_{3/2}^3]_1 3d_{5/2}$	$\frac{5}{2}$	1.6585[3]	8.139[12]
48	$2s^22p^4(^3P)3d\ ^2F$	$[2s^22p_{1/2}2p_{3/2}^3]_1 3d_{3/2}$	$\frac{5}{2}$	1.6601[3]	1.562[13]
49	$2s^22p^4(^1D)3d\ ^2P$	$[2s^22p_{1/2}2p_{3/2}^3]_1 3d_{5/2}$	$\frac{3}{2}$	1.6607[3]	3.638[11]
50	$2s^22p^4(^1D)3d\ ^2G$	$[2s^22p_{1/2}2p_{3/2}^3]_2 3d_{3/2}$	$\frac{7}{2}$	1.6652[3]	
51	$2s^22p^4(^1D)3d\ ^2G$	$[2s^22p_{1/2}2p_{3/2}^3]_2 3d_{5/2}$	$\frac{9}{2}$	1.6669[3]	
52	$2s^22p^4(^1D)3d\ ^2D$	$[2s^22p_{1/2}2p_{3/2}^3]_2 3d_{5/2}$	$\frac{5}{2}$	1.6696[3]	4.870[13]
53	$2s^22p^4(^1D)3d\ ^2S$	$[2s^22p_{1/2}2p_{3/2}^3]_2 3d_{3/2}$	$\frac{1}{2}$	1.6701[3]	2.643[12]

TABLE I. (*Continued*).

Level	*LS* state	*jj* state	*J*	Energy (eV)	A^r (s^{-1})
54	$2s^22p^4(^1D)3d\ ^2F$	$[2s^22p_{1/2}2p^3_{3/2}]_2 3d_{5/2}$	$\frac{7}{2}$	1.6729[3]	
55	$2s^22p^4(^1D)3d\ ^2D$	$[2s^22p_{1/2}2p^3_{3/2}]_2 3d_{3/2}$	$\frac{3}{2}$	1.6734[3]	5.796[13]
56	$2s^22p^4(^1D)3d\ ^2F$	$[2s^22p_{1/2}2p^3_{3/2}]_2 3d_{3/2}$	$\frac{5}{2}$	1.6749[3]	6.264[13]
57	$2s^22p^4(^3P)3d\ ^2D$	$[2s^22p_{1/2}2p^3_{3/2}]_2 3d_{5/2}$	$\frac{3}{2}$	1.6823[3]	1.593[13]
58	$2s^22p^4(^1D)3d\ ^2P$	$[2s^22p_{1/2}2p^3_{3/2}]_2 3d_{5/2}$	$\frac{1}{2}$	1.6847[3]	1.343[13]
59	$2s^22p^4(^3P)3d\ ^4P$	$[2s^22p^4_{3/2}]_0 3d_{5/2}$	$\frac{5}{2}$	1.7175[3]	4.115[11]
60	$2s2p^53s$			1.7191[3]	
61	$2s^22p^4(^1S)3d\ ^2D$	$[2s^22p^4_{3/2}]_0 3d_{3/2}$	$\frac{3}{2}$	1.7218[3]	3.334[10]
62	$2s2p^53p$			1.7708[3]	4.762[12]
63	$2s2p^53d$			1.8322[3]	
64	$2s^22p^44l$			2.1018[3]	1.770[12]

lump the two multiplet levels and treat them as one single level, as shown in Fig. 1. The combined model shown in Fig. 1 includes all the important processes responsible for line formation from the $n=3$ states in a compact fashion designed to minimize some of the burden of dealing with a superabundance of atomic data and energy levels. Recently, the advent of supercomputers and the availability of sophisticated atomic codes [22–32] have made it possible to generate and handle large numbers of level structures efficiently for atomic modeling. However, while it is important to lump most multiplets into configuration states to achieve this efficiency, it is also important to represent some charge states with sufficient sublevels to allow detailed analysis of diagnostically important emission processes [14]. The remaining number of important configuration levels and the rest of the ionization stages can then be treated in a less detailed way, albeit resulting in approximations in the coupling of the averaged ionization levels with the detailed levels and in the formulation of the rate equations.

Specifically, the Se XXV model consists of 31 states including the ground level; the 26 fine-structure levels of the $n=3$, $2p^53s$, $2p^53p$, and $2p^53d$, configurations, three lumped inner-shell $n=3$ configurations; $2s2p^63s$, $2s2p^63p$, and $2s2p^63d$; and a lumped $n=4$ level [21]. For Se XXVI, we have updated the model used in Ref. [21] by including all 57 fine-structure levels for the $n=3$ singly excited states. Thus the Se XXVI stage contains a lumped ground state; a $\Delta n=0$ excited state, 57 fine-structure levels of the $2p^43s$, $2p^43p$, and $2p^43d$ configurations; three lumped inner-shell excited configurations; $2s2p^53s$, $2s2p^43p$, and $2s2p^43d$; and a lumped $n=4$ state (see Table I). As mentioned above, the Se XXVI and Se XXV models are then embedded in a detailed configuration accounting atomic model of selenium [33] from which an ionization balance can be calculated. The model in Ref. [33], for example, contains the level structure for Se XXIV that we have used consisting of the $2p^63s$ ground state, the lumped $n=3$ singly excited state (namely, $2p^63p$ plus $2p^63d$), and lumped configuration averaged states for $4\leqslant n\leqslant 6$ excited states. The $n=3$ singly excited states for both Se XXVI and Se XXV ions are fully coupled (to the ground states above and below and among themselves and the other excited states). Each population within the $n=3$ multiplet, which together are responsible for resonance line cluster formation, can be calculated and departures from *local thermodynamic equilibrium* (LTE) behavior can be determined.

Satellite lines, formed on the long wavelength sides of the resonance lines for high Rydberg levels, are often blended with the resonance lines. Thus the autoionizing configurations $2p^43lnl'$ of Se XXV and $2p^53lnl'$ of Se XXIV with $n=3$ which form the spectroscopically isolated satellites as well as configurations with $n\geqslant 4$ that form unresolved satellites are also included in our model. After simultaneous calculations of the populations of all ionization stages surrounding the Se XXVI and Se XXV ionization stages, and all populations of the Se XXVI and Se XXV states, shown in Fig. 1, are performed, the populations of doubly excited states are obtained by post-processing the ground and singly excited state populations of the CRE calculations.

The following line formation mechanisms are considered in our calculations. For the resonance lines, the most dominant contributions come from direct electron-impact excitation from the ground state. We have included direct collisional excitations, deexcitations, and radiative decay from or to the ground states and from cascades through the $n=3$ inner shell and $n=4$ states of Se XXVI and Se XXV. Additional contributions due to resonance excitations (RE's), in which the upper levels of the resonance lines are formed by the autoionization decay of doubly excited (DBEX) states, are included along with direct excitation for the $n=3$ excited states of Se XXV. All collisional ionizations from excited states of both F- and Ne-like ionization stages to the ground states of the O- and F-like states, respectively, are included in this work. However, no inner-shell ionizations that directly connect excited states were included. All possible radiative and collisional couplings among the $n=3$ fine-structure levels of Se XXVI and Se XXV are also included in this analysis. The excited states are substantially populated by DR, and we have included a detailed state specific contribution of DR for recombination from the ground and $\Delta n=0$ states of Se XXVII and Se XXVI to the $n=3$ singly excited states of Se XXVI and Se XXV, respectively. The contributions from the DR satellites due to high Rydberg levels that are unresolved from the resonance lines may have important consequences [34], and we examine whether they must be taken into account in order to compare calculated line ratios with experiments. Some of the previous diagnostic models contained inaccuracies because they lacked these

necessary theoretical considerations in their calculations and experimental refinements [35–38].

Data for the atomic processes involved in populating or depopulating the levels that are included in this calculation was obtained as follows:

(i) Direct and resonance collisional excitation. Electron-impact collision strengths for excitation from the ground to all the excited states and collisional coupling among all the excited Se XXVI levels were calculated by using the relativistic atomic structure and distorted wave (RDW) codes of Refs. [22–25]. The collision strengths calculated for the $n=2$-3 excitations were compared to those published by Sampson, Zhang, and Fontes [24]. For Se XXV, collision strengths for excitation from the ground state were obtained from Zhang and co-workers [27,39] and the collisional couplings among the $n=3$ levels were obtained from Hagelstein and Jung [32]. The excitation collision strengths from the ground as well as from the nl states with $n=3$ configurations to the lumped $n=4$ states of both Se XXVI and Se XXV ions were calculated by using a modified version of the atomic structure code of Cowan [29], called CATS [30] and a distorted wave code, called ACE [31] for each $4l$ configuration and then they were added to obtain a total collision strength. The collision excitation rate coefficients were then obtained by fitting the collision strength data points and using the fits to integrate them over a Maxwellian electron distribution. The distorted-wave rate coefficients for electron-impact excitations of the inner-shell excited Ne- and Na-like satellite lines were calculated by using ACE for the range of temperatures needed for this work. Besides direct collision excitation, resonance excitations (RE's) of the $n=3$ singly excited states of Se XXV, which begin with a radiationless capture into DBEX Se XXIV states of the form $3lnl'$ $(n\geqslant 7)$ and $4l4l'$ and then end with autoionization to the singly excited states of Se XXV, are also included in the ionization calculation. Radiative decay channels from the DBEX states lead to recombination to the Se XXIV states. The contribution due to RE's to the $3s$ levels is much larger than that due to direct excitation. These RE branching ratios were calculated in the resonance approximation following Cowan [40].

(ii) Collisional ionization. Electron-impact ionization cross sections for ionization from the ground as well as from all the excited Se XXVI states were also calculated relativistically from the RDW ionization code of Refs. [26] and [28]. For Se XXV, the collision ionization rates from the $3s$, $3p$, and $3d$ levels were obtained from Golden, Sampson, and Omidvar [41] and Moores, Golden, and Sampson [42]. The collisional ionization cross sections from the $n=4$ configurations were obtained using the CATS [30] code. Ionization cross sections were also scaled, and rate coefficients were calculated by integrating them over a Maxwellian distribution for each required temperature.

(iii) Radiative and dielectronic recombination. A detailed and comprehensive description of the methodology involved in computing the DR rates is described in the work by Dasgupta and Whitney [43]. DR data for recombination from Se XXVI to singly excited states of Se XXV [43] and from Se XXVII to singly excited states of Se XXVI [44] were calculated using the Hartree-Fock with relativistic method of Cowan [29]. Detailed calculations were carried out for DR branching ratios and rates from the ground and $\Delta n=0$ states of Se XXVII and Se XXVI to each specific fine structure levels of Se XXVI and Se XXV, respectively. For low lying DBEX states, DR branching ratios were explicitly calculated, while for higher Rydberg states a $1/n^3$ falloff extrapolation of the DR branching ratios was used. Here n denotes the principal quantum number of the Rydberg electron that participates in the recombination process. Only total ground-to-ground radiative recombination couplings of the Se XXVII to Se XXVI and Se XXVI to Se XXV ionization stages were included in our model. However, three-body recombination to each excited state as well as the ground state was included in the calculations. These rates were obtained by detailed balancing the collisional ionization rate coefficients.

(iv) Spontaneous radiative decay. Oscillator strengths and radiative decay rates for all 62 Se XXVI excited levels were calculated from the DFW atomic code of Sampson *et al.* [22]. For Se XXV, oscillator strengths were obtained from Cowan [29]. These oscillator strengths were then used to calculate the spontaneous radiative transition probabilities for all the level to level transitions from and to the $n=3$ levels. Radiative transition probabilities from the lumped $n=4$ states to the ground and to $n=3$ states were obtained by statistically averaging the multiplet probabilities.

(v) Collisional couplings and cascades. We have incorporated collisional excitation and deexcitation rates among all levels in our Se XXVI and Se XXV models. The rates from the $n=4$ lumped states to all lower $n=3$ multiplet states were obtained from the individual J-J' rates with the assumption that the populations of the individual upper J levels are statistically distributed. The same assumption was made in obtaining the collisional ionization and radiative decay rates from the $n=4$ states. Except at very low densities, this assumption is generally more reasonable for the more closely spaced and strongly coupled $n=4$ states than it is for the $n=3$ states. Collisional and radiative cascades from the $n=4$ and the $n=3$ states to all lower states are included in the atomic model and CRE solutions. However, radiative cascades among autoionizing levels for the determination of DR and RE rates were neglected in our calculations. Also, collisional or radiative cascades from singly excited levels higher than $n=4$ were not included in this calculation.

III. IONIZATION EQUILIBRIUM RESULTS

A. Resonance line ratios

In general, population densities of ground and singly excited states are obtained by solving a set of rate equations of the form

$$\frac{df_\mu}{dt}=\sum_{\nu\neq\mu} W_{\mu\nu}f_\nu-\sum_{\nu\neq\mu} W_{\nu\mu}f_\mu, \tag{1}$$

where $f_\mu=N_\mu/n_i$ (with $n_i\equiv\Sigma N_\mu$) is the fractional population of the level μ, and $W_{\mu\nu}$ are the sums of all rates populating level μ from level ν. Steady-state population densities are obtained by solving the inequilibrium equations, $df_\mu/dt=0$.

In the ion density region of interest for the present calculations, $10^{18}\leqslant n_i\leqslant 10^{22}$, the plasma ionization condition cannot be described by *corona equilibrium*, in which radiative decay rates are much larger than collisional excitations,

and essentially all ions exist in the ground and $\Delta n=0$ levels. Neither can the plasma be described as being in LTE, where all states of a given configuration are statistically populated. In the intermediate density region, $10^{18} \leqslant n_i \leqslant 10^{22}$ cm^{-3}, the $n=3$ states of Se XXVI and Se XXV are nonstatistically distributed. Only at densities above 10^{22} cm^{-3} do these sublevels come into statistical equilibrium. In this paper, we will present equilibrium solutions to the rate equations, which contain all of the level-to-level transitions described above. The nonstatistical behavior of the $n=3$ L-shell states provides the basis for using resonance line emissions from these states for selenium plasma diagnostics.

The x-ray spectrum for Se XXV consists of seven allowed transitions from the $n=3$ states to the closed $^1S_0$ ground state. Of these lines, which are identified as $3A(^1S_0\text{-}2s2p^6 3p\ ^1P_1)$, $3B(^1S_0\text{-}2s2p^6 3p\ ^3P_1)$, $3C(^1S_0\text{-}2s^2 2p^5 3d\ ^1P_1)$, $3D(^1S_0\text{-}2s^2 2p^5 3p\ ^3D_1)$, $3E(^1S_0\text{-}2s^2 2p^5 3d\ ^3P_1)$, $3F(^1S_0\text{-}2s^2 2p^5 3s\ ^3P_1)$, and $3G(^1S_0\text{-}2s^2 2p^5 3s\ ^3P_1)$, the less intense $3E$ line is blended with a Se XXIV satellite line. The fluorine spectrum is more complicated, having many allowed $2p^5\text{-}2p^4 3s$ and $2p^5\text{-}2p^4 3d$ transitions that lie between the $3B$ and $3C$ lines and the $3D$ and $3F$ lines of Se XXV, respectively. In particular, they are difficult to analyze individually unless they are observed and identified with very high resolution. Some of these lines also overlap with some of the long wavelength lines of Se XXVII. Even when the overlapping Se XXVII lines are less intense, it is imperative that they be identified and excluded from the Se XXVI resonance lines, if possible, for comparisons with the theoretical calculations of this paper to be made.

In order to minimize some of these difficulties, this present diagnostic work involves the analysis of clusters of strong resonance and satellite lines. Specifically, we will consider the $2p$-$3s$, $2p$-$3d$, and $2s$-$3p$ resonance clusters and their satellites for both ions. We begin with a discussion involving the resonance lines alone. Since the Se XXV ground state is a closed shell, there are only the seven allowed resonance transitions that are listed above. These lines, along with their satellites, are more readily identified and detected than the Se XXVI lines, since the Se XXVI spectrum has 34 allowed transitions of the $2p^5\text{-}2p^4 3d$ type alone lying between the $2p$-$3d$ and $2s$-$3p$ Se XXV lines. It also has 14 $2p^5\text{-}2p^4 3s$ transitions lying between the $2p$-$3d$ and $2p$-$3s$ Se XXV lines. Experimentally, diagnostic work is based on integrations under the lines of a spectrum. It requires either that individual lines be isolated or that, when they overlap, line clusters be isolated as best possible. In the latter case, integration errors are reduced because the integration is over the broader range of energies that are contained within a cluster.

For both the Se XXVI and Se XXV resonance lines, therefore, we will sum lines originating from the same configuration as the clusters under consideration. All of the lines of the $2p(J)$-$3s(J')$ resonance transitions are denoted by the single transition, $2p$-$3s$, and the same treatment is followed for $2p$-$3d$ and $2s$-$3p$ transitions. We do the same lumping when we consider the satellites to these resonance lines. The $2p$-$3d$ and $2p$-$3s$ line clusters for Se XXVI and Se XXV are nonoverlapping; hence intensity ratios involving these lines should be useful for plasma diagnostics.

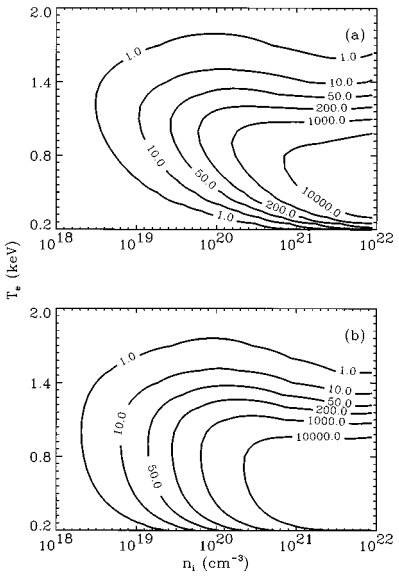

FIG. 2. Power contours for the $2p$-$3d$ resonance lines: (a) Se XXVI, (b) Se XXV. These resonance line clusters include the contributions due to unresolved satellites.

Power densities emitted by the strong $2p$-$3d$ resonance lines for both Se XXV and Se XXVI are functions of n_i^2, and range over eight orders of magnitude in the density range under consideration. Contours for these optically thin powers per unit volume, which are shown in Fig. 2, are given by

$$P_{R(\mathrm{F/Ne})} = \sum_j N^*_{j(\mathrm{F/Ne})} A_r(j \rightarrow g) E_{jg}\,, \tag{2}$$

where N_j^* is the population of an upper $3d$ level $|j\rangle$ of the F- or Ne-like line, $A_r(j \rightarrow g)$ is the radiative decay rate from level $|j\rangle$ to the ground level $|g\rangle$, and E_{jg} is the energy for this transition. Both of the power contours in Fig. 2 have similar temperature and density dependences; a maximum occurs as a function of temperature at a temperature that decreases with increasing density. As the temperature increases, the power declines after the maximum is passed because the excited state populations are depleted by ionization to the higher ionization stages. Moreover, as one would expect for a closed-shell system, the power emitted from the Se XXV $3d$ configuration is larger over the same density and temperature range than it is for Se XXVI.

The dependence of the populations of the $3d$ configurations on both density and temperature are shown in Fig. 3. As the density increases, the $3d$ states are populated more and more from collisional deexcitations from the upper levels, but they only begin to equilibrate at ion densities close to 10^{22}. This behavior is illustrated in Fig. 4 for two metastable and two spontaneously decaying $3d$ states of Se XXVI. This figure shows the fractional populations within the $3d$ configuration that are calculated as a function of density at a fixed temperature of 800 eV. At low densities, $3d$ populations are stored essentially in the metastable states. At the high density, 10^{22} cm^{-3}, the fractional populations have achieved their LTE values $g_J/\Sigma_J g_J$, where $g_J=2J+1$ is the statistical weight of the state. As the temperature increases, the plasma ionizes through several ionization stages and the

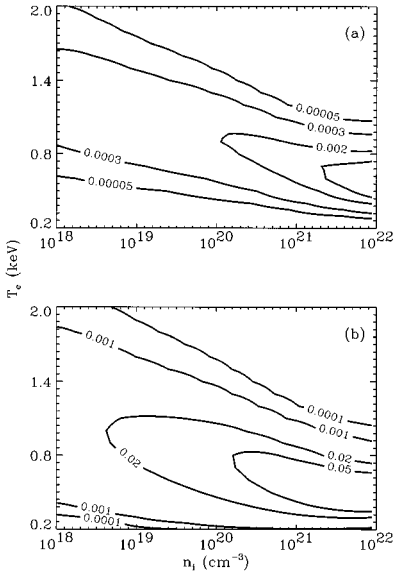

FIG. 3. Contour plots of the total fractional population for the $3d$ configurations, which are obtained by adding the populations of all the individual multiplet levels for these configurations: (a) Se XXVI, (b) Se XXV. The unlabeled contour in (a) has the value of 0.005.

population of the $3d$ states for both Se XXV and Se XXVI decreases due to this ionization. However, since there is a large abundance of Se XXV ground states in CRE to collisionally excite the Se XXV $3d$ states, they have relatively larger populations compared to the Se XXVI $3d$ states.

Since populations of the ground as well as the excited states are self-consistently obtained using all the relevant atomic processes connecting these levels in the CRE calculation, the intensities of line emission that are calculated from the excited states have self-consistent temperature and density dependences in the same range as the populations. From these intensities, one can obtain the contour plots of resonance line cluster (or configuration) ratios shown in Figs. 5–8. Since temperature is plotted along the vertical axis and ion density along the horizontal axis, contours of quantities

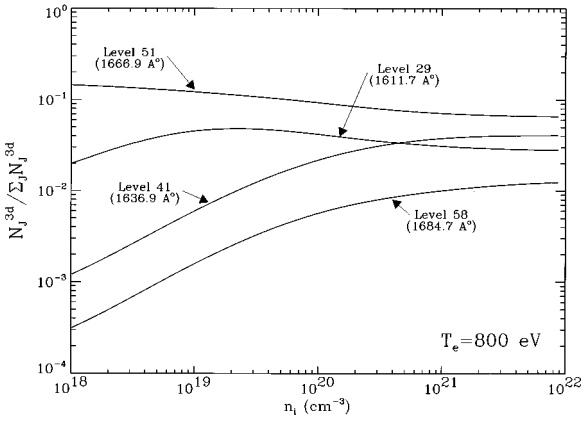

FIG. 4. Fractional occupation of two metastable and two spontaneously decaying $3d$ states of Se XXVI as a function of density at T_e=800 eV. The levels are identified in Table I. This figure shows how the relative populations reach their LTE values around n_i= 10^{22} cm^{-3}.

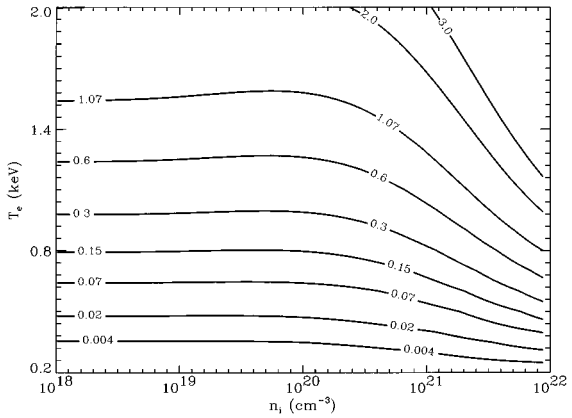

FIG. 5. Contour plots of the Se XXVI to Se XXV ratios of the $2p$-$3d$ line clusters. These resonance line clusters include the contributions due to unresolved satellites.

that are mostly parallel to the horizontal axis are primarily temperature sensitive, while density sensitivity shows up as mostly vertically running contours. Figure 5 shows the contours of the $2p$-$3d$ Se XXVI to Se XXV ratios. These ratios have strong temperature dependences, and become density sensitive only at high densities. However, as the ratios increase with increasing temperature, the contours become density sensitive at lower and lower densities. The density sensitivity at high densities is due to collisional deexcitations which influence the $3d$ populations comparably to the radiative decay rates of these states. Although similar behavior is observed for the $2p$-$3s$ line ratios of the two ions, the ratios of $2s$-$3p$ lines show the most density sensitivity even at lower densities.

The resonance-to-resonance line ratios, $2p$-$3s$ to $2p$-$3d$, within both Se XXVI and Se XXV ionization stages, are quite sensitive to density. This sensitivity has been experimentally observed and theoretically explained [17] in Ne-like bromine in a laser-produced plasma. As seen in Fig. 6, the $2p$-$3s$ to

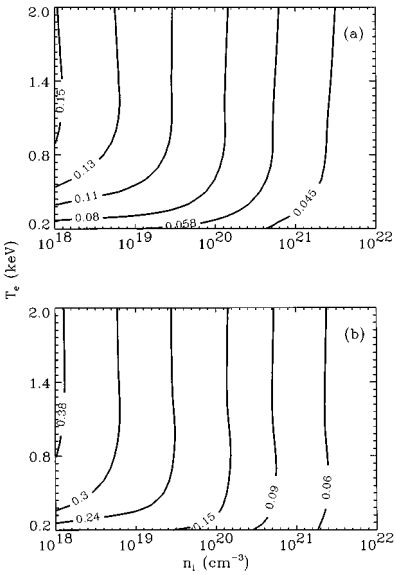

FIG. 6. Contour plots of the $2p$-$3s$ to $2p$-$3d$ resonance to resonance line cluster ratios for (a) Se XXVI and (b) Se XXV. These lines include all the contributions due to unresolved satellites.

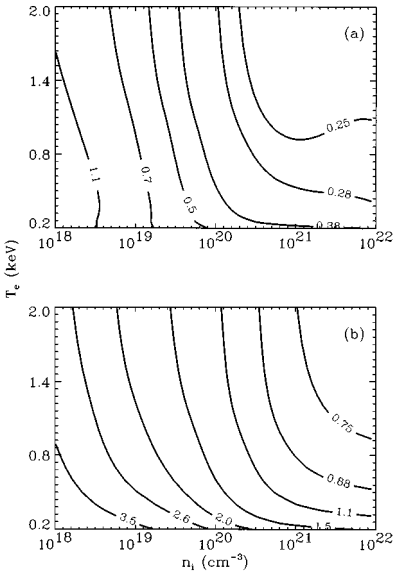

FIG. 7. Contour plots of the $2p$-$3s$ to $2s$-$3p$ resonance to resonance line cluster ratios for (a) Se XXVI and (b) Se XXV. These lines include all the contributions due to unresolved satellites.

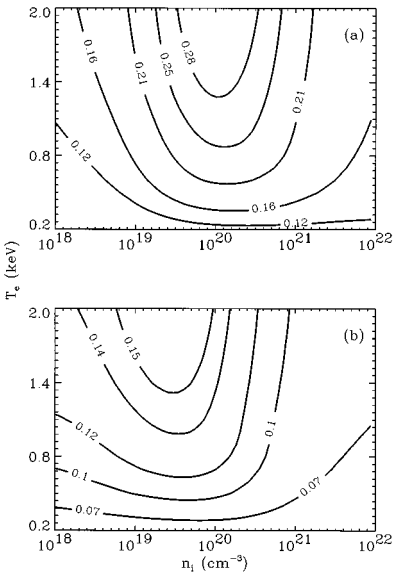

FIG. 8. Contour plots of the $2s$-$3p$ to $2p$-$3d$ resonance to resonance line cluster ratios for (a) Se XXVI and (b) Se XXV. These lines include all the contributions due to unresolved satellites.

$2p$-$3d$ cluster ratios for both Se XXVI and Se XXV are mostly vertical for the higher temperatures and densities, while for lower temperature the contours tend to move toward lower densities. This behavior can be explained by examining the population dynamics of the excited states. At low electron densities and temperatures, most of the configuration population is in the $2p^q3s$ and $2p^q3p$ configurations. Most of these states are populated by collisions from the ground state and radiative cascades from higher-lying excited states. As the density increases, the population of the singly excited $2p^q3d$ configuration, which is also populated by direct collisional excitation, increases due to additional collisional excitations and deexcitations to these states. Thus the $2p$-$3s$ to $2p$-$3d$ line ratios are density sensitive and the density dependence gets weaker with increasing density. Also, in contrast to the $3d$ levels, the $3s$ levels for both Se XXVI and Se XXV are populated more by DR than by direct collisional excitation. Since the mechanisms of collisional excitation and DR are from different ion states, the $2p$-$3s$ to $2p$-$3d$ line ratios depend on the ion density.

This density dependence of the resonance lines is most pronounced in the $2p$-$3s$ to $2s$-$3p$ ratios as shown in Fig. 7. The $2s2p^{q+1}3p$ states, which receive relatively less population from direct collisional excitation from the ground state, become strongly populated due to transfer of populations of metastable excited levels due to collisions at higher densities. The contours of these line ratios at higher densities tend to move toward higher densities in contrast to those of the $2p$-$3s$ to $2p$-$3d$ line ratios. Along with their density dependence, the $2s$-$3p$ to $2p$-$3d$ line ratios show a strong temperature dependence, especially at low temperatures as shown in Fig. 8. The ''u'' shapes of the contours of these line ratios indicate opposite variations of these line ratios at high densities compared to that at low densities. The fact that we have treated the inner-shell $n=3$ excited states in a configuration average approximation might result in some inaccuracies in calculating line intensities involving these states. The results of the calculated population with a fine-structure level model and a lumped configuration level model are different, because the total radiative transition probabilities of the fine-structure levels, some of which are metastables, is different than the radiative transition probability of the lumped state. Thus the $2p$-$3s$ to $2s$-$3p$ and $2s$-$3p$ to $2p$-$3d$ resonance to resonance line ratios may be more density dependent at low densities than shown in Figs. 7 and 8, respectively. We have treated the inner-shell $n=3$ excited states in the configuration average approximation consistently with the explicit multiplet treatment of other $n=3$ singly excited states. This approximation allows us to take ratios of the $3p$ inner-shell lines that involve the full cluster of inner-shell transitions. There is some error involved in this procedure; however, it is expected that lumping of the $2s$ hole states will not affect the line ratios as significantly for these states as it would for the valence electron $n=3$ states, since the hole states are higher lying and their level splittings are smaller. Thus the hole-state subpopulations deviate by smaller amounts from statistical equilibrium than those of the valence electron states.

B. Satellite line effects

We next examine the degree to which unresolved satellite lines influence these cluster powers and power ratios. The satellite structures to the Se XXVI $2p$-$3d$ and $2p$-$3s$ resonance lines consist of a large number of lines whose individual detection is difficult, if not impossible, even with extreme high experimental spectral resolution. Satellite lines are formed on the long wavelength sides of the resonance lines when the spectator electron is in an $n=3$ state of the DBEX states that are formed by the DR process. For the $n\geqslant 4$ states, the satellite lines are often blended with the resonance lines. Se XXV and Se XXIV satellite lines are formed following dielectronic capture from the ground states of Se XXVI and Se XXV to the $3l3l'$ DBEX states, which then decay to the $n=3$ singly excited states of each recom-

bined ion. These satellite lines can also be formed by the alternative mechanism of direct excitation of an inner-shell (ISE) electron of an excited ion such as the $\Delta n=0$ state of Se XXIV for satellites to the Se XXV resonance lines. In this work, we have considered only inner-shell excitations from the $n=3$ levels for satellite formation, and neglected any excitation contributions from higher excited levels. The contribution due to ISE's as compared to DR is expected to be of no significance for low-Z ions in steady-state calculations. Since the contribution of an ISE to the intensities of satellite lines becomes more important for ions with moderately higher Z, we have investigated both DR and ISE contributions to the formation of Se XXV and Se XXVI satellite lines. The populations of the upper levels involved in satellite line formation due to DR and ISE's are calculated as separate contributions.

When the resonance line intensities are corrected for unresolved dielectronic satellites from the $n\geqslant 4$ DBEX states, Eq. (2), for example, is modified to

$$P'_{R(\mathrm{F/Ne})}=P_{R(\mathrm{F/Ne})}+N_{g(\mathrm{F/Ne})}\sum_{j'k}\left[N_e\sum_i\ \alpha_{\mathrm{DR}}(i,j',k)E^{**}_{j'k}\right], \tag{3}$$

where N_e is the electron density and, in this restricted sum, $E^{**}_{j'k}$ ($\cong E_{ji}$) is the transition energy from the DBEX states j' to the recombined levels k, and

$$\alpha_{\mathrm{DR}}(i,j',k)=\left[\frac{4\pi\mathcal{R}}{kT}\right]^{3/2}\frac{a_0^3}{2g_i}\sum_{j'}\ F_{ij'k}\exp(-\varepsilon_{j'}/kT), \tag{4}$$

is the DR rate coefficient where the DR branching ratio $F_{ij'k}$ is defined by

$$F_{ij'k}\equiv\frac{g_{j'}A^A_{j'i}A^R_{j'k}}{\sum_{i'}\ A^A_{j'i'}+\sum_{k'}\ A^R_{j'k'}}. \tag{5}$$

In Eq. (4), $\varepsilon_{j'}$ is the energy of the autoionizing state with respect to the initial state; $|i\rangle$ which can be either the ground or the $\Delta n=0$ state for Se XXVI, and g_i and $g_{j'}$ are the statistical weight factors of the states $|i\rangle$ and $|j'\rangle$, respectively; a_0 is the Bohr radius; and $\mathcal{R}$ is the Rydberg energy. The summations in Eq. (5) are carried over all possible autoionized states $|i'\rangle$ (including autoionizations to excited states), and all possible final recombined states $|k'\rangle$ that are the lower levels for the satellites to the $3d$ states.

The inclusion of unresolved satellite lines to the total power emitted by the strong $2p$-$3d$ resonance lines of Se XXV and Se XXVI can be quite significant especially at high densities. This effect is shown in Fig. 9 for $T_e=500$ eV. However, when contour plots of the resonance line powers, both with and without satellite contributions, are compared over the entire density and temperature range of our calculations, the contributions of the unresolved DR satellite lines to the line intensities are generally negligible. One can anticipate that these contributions should become increasingly important in high density plasmas, when collisional mixing of the DBEX states occurs and the population of the $n=4$ states is increased by this mixing.

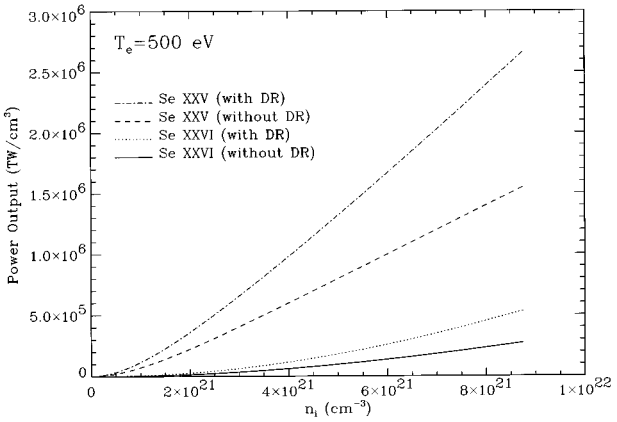

FIG. 9. Total power emitted from the strong $2p$-$3d$ resonance line clusters of Se XXVI and Se XXV. The effects of the contributions due to unresolved dielectronic satellites are shown as solid for Se XXVI without DR; dotted for Se XXVI with DR; dashed for Se XXV without DR; and dash-dotted for Se XXV with DR. The DR contribution to the resonance lines become significant only at high densities.

While some satellite lines blend with the resonance lines and contribute directly to the intensity of such lines, other satellites formed by electron capture to low Rydberg states with $n=3$ can be spectroscopically resolved from the parent resonance lines. The power emitted per unit volume from such satellites to either F- or Ne-like lines is

$$P_{S(\mathrm{F/Ne})}=N_e\left[\sum_{ij'k}N_{g(\mathrm{F/Ne})}\alpha_{\mathrm{DR}}(i,j',k)+N^*_{\mathrm{Ne/Na}}C_{\mathrm{ISE}}\frac{A^R_{j'k}}{\sum_{i'}\ A^A_{j'i'}+\sum_{k'}\ A^R_{j'k'}}\right]E^{**}_{j'k}, \tag{6}$$

where $N^*_{\mathrm{Ne/Na}}$ is the population of the excited states, and C_{ISE} is the inner-shell excitation rate coefficient. The branching ratio term in Eq. (6) arises because, in addition to forming a satellite line by undergoing a radiative decay to a stabilized excited state, the DBEX states also decay by the competing processes of autoionization and radiative decays to other excited states. Since the satellites formed due to ISE come mostly (and solely in case of satellites to Se XXVI lines) from the excited states that have maximum values at much lower temperatures compared to the temperatures at which C_{ISE} has large values, the power emitted due to line formation by ISE in CRE is found to be much smaller than due to DR.

Satellite line ratios of two different ions can be used for plasma diagnostics in the same way as resonance line ratios of different ions of the same element. Lunney [45], for example, proposed the use of He- and Li-like DS line ratios to measure electron temperature and the state of ionization for high-density laser-produced and z-pinch plasmas. However, in the L shell, where the multiplet structures are more complex and energy splittings are larger, we see a different result. When we calculate the intensity ratio of all the lines that

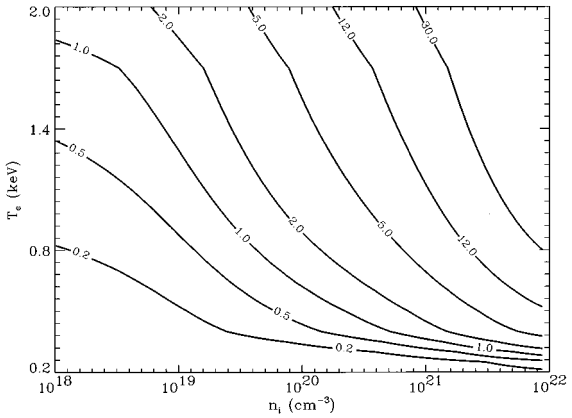

FIG. 10. Contour plots of the Se XXVI to Se XXV ratios of satellite line clusters to the $2p$-$3d$ resonance line. These ratios become more density sensitive when contributions due to ISE are included in the calculation of satellite intensities.

are satellite to the $2p$-$3d$ resonance lines of Se XXVI to the similar set of satellites to the $2p$-$3d$ lines of Se XXV, and make a contour plot of the results, we find that the contours are more vertical than horizontal. Therefore, this line ratio is more density sensitive compared to the parent resonance line ratios (as shown in Fig. 5) and more density sensitive than temperature sensitive. The contour plots of this satellite intensity ratio are shown in Fig. 10. As expected, the density sensitivity decreases when contributions due to ISE are excluded from the calculation since, when line ratios are dependent on more ion fractions (and ISE and DR involve two different initial ion stages), they become more density sensitive. However, in the case under study, even when the dielectronic satellite lines are due to line emissions from DBEX states populated only by the DR process, the ratio of satellite structures from neighboring ionization stages is density sensitive.

Ratios of satellites to resonance lines, on the other hand, are strongly temperature dependent, and routinely used for temperature diagnostics for laboratory and astrophysical K-ion plasmas. This temperature sensitivity comes about because the electron energies responsible for a multiplet of DS and resonance lines sample different parts of the electron distribution function. Figure 11 shows contours of satellite-to-resonance line cluster ratios that were calculated for the $2p$-$3d$ lines within Se XXVI [Fig. 11(a)] and Se XXV [Fig. 11(b)]. These line ratios show a similar density sensitivity to the one seen in the ratio of $2p$-$3s$ to $2p$-$3d$ resonance lines. They tend to become more density dependent as density increases. This density sensitivity can be understood from Fig. 4. As the density is increased, the metastable $3d$ states share more of their population with the radiating $3d$ states until a LTE distribution of states is reached. The $3d$ radiation rate increases correspondingly. In addition, as the density increases, angular-momentum-changing electron-ion collisions can redistribute the populations of the DBEX states, and this causes increases in the intensity of the satellite lines, especially those coming from upper levels that are metastable to autoionizations [46]. Zigler *et al.* [4] used these density-enhanced dielectronic satellite lines to diagnose plasma electron densities. However, we have not included this effect of angular momentum changing electron-ion collisions redis-

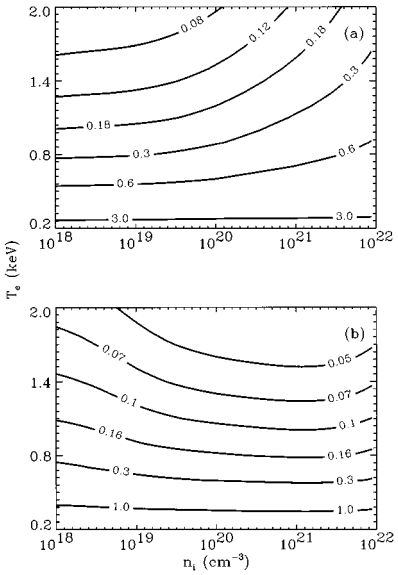

FIG. 11. Contour plots of ratios of $2p$-$3d$ satellites to resonance lines for (a) Se XXVI and (b) Se XXV. The satellite lines include the contributions due to ISE.

tributing the DBEX states in our calculation. Also, even though the ratio of dielectronic satellites formed by DR to resonance lines are mostly temperature dependent because the excitation fluxes of both the satellites and the resonance lines can come substantially from the same ionization state, when ISE contributions to the satellites are included in the line ratios, density dependences of the ratios arise. This can be seen by comparing the line ratios of Fig. 11(a) with Fig. 12(a) and Figs. 11(b) with Fig. 12(b), where Figs. 12(a) and 12(b) exclude ISE contributions to the satellites.

The intersection of contours that are almost vertical with contours that are mostly horizontal can be used for making a simultaneous diagnostic of both an electron temperature and an ion density. Mostly horizontal, temperature-sensitive, contours are provided by the line ratios of the $2p$-$3d$

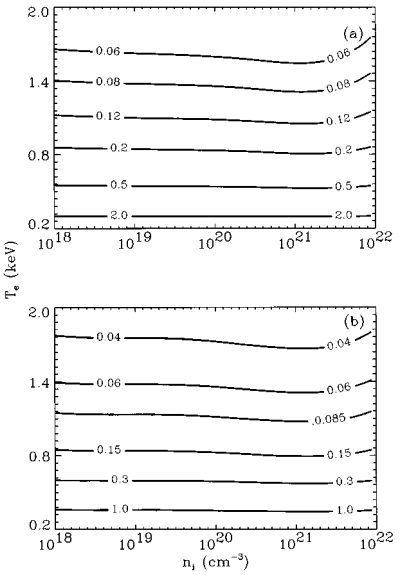

FIG. 12. Same as Fig. 11, except there is no ISE contributions to the satellite line intensities.

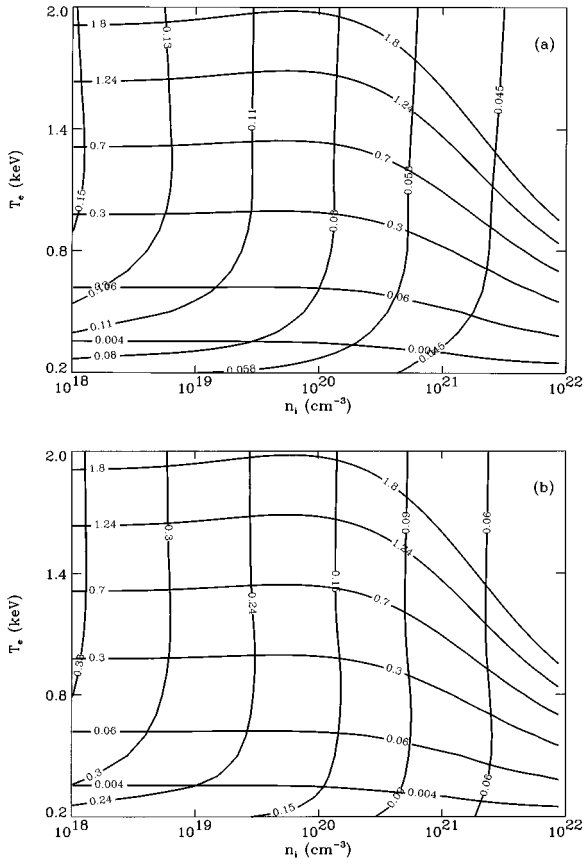

FIG. 13. Overlap of mostly temperature sensitive contours of Se XXVI to Se XXV ratios of $2p$-$3d$ line clusters (Fig. 5) and mostly density sensitive contours of $2p$-$3s$ to $2p$-$3d$ resonance to resonance line ratios for (a) Se XXVI [Fig. 6(a)] and (b) Se XXV [Fig. 6(b)]. Intersecting points of these two plots determine the temperature and density simultaneously.

resonance-plus-satellite lines of Se XXVI to those of Se XXV (similar to those shown in Fig. 5). Mostly vertical, density-sensitive, contours are provided by the $2p$-$3s$ to $2p$-$3d$, resonance-plus-satellite, intraion line ratios involving either Se XXVI or Se XXV [similar to those shown in Figs. 6(a) and 6(b), respectively]. These two sets of contours are shown in Figs. 13(a) and 13(b). By attempting to fit both ratios simultaneously on both figures, one determines an electron temperature and an ion density that is consistent with three of the major features of the emission spectrum. If a significant disagreement occurs between the inferences drawn from Fig. 13, then one can conclude that either the optically thin or the CRE assumption is invalid, or that both are.

An example of an application of this procedure can be provided by an analysis of the experimental spectrum published in Ref. [47]. A numerical integration of this spectrum produces the following estimate of the line ratios plotted in Fig. 13. The Se XXVI to Se XXV $2p$-$3d$ line ratio obtained from this analysis was 1.24 and the $2p$-$3s$ to $2p$-$3d$ line ratios for Se XXVI and Se XXV were 0.34 and 0.47, respectively. In trying to locate these points (1.24,0.34) in Fig. 13(a) and (1.24,0.47) in Fig. 13(b), we find that they place the spectrum well outside the density range shown in Figs. 13(a) and 13(b), i.e., approximately $T_e \sim 1.65$ keV and the density estimate lies well below 10^{18} cm^{-3}. However, both

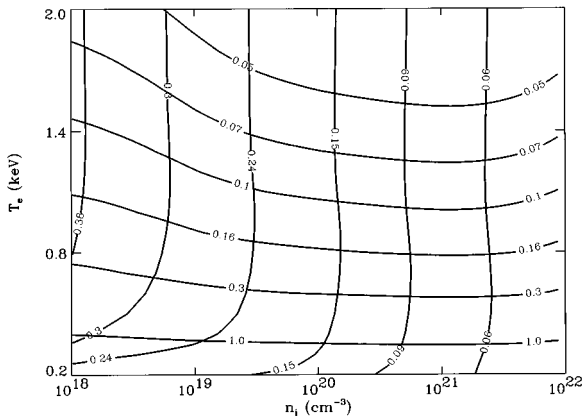

FIG. 14. Overlap of contours of satellite to $2p$-$3d$ resonance line cluster ratios of Se XXV [Fig. 11(b)] and contours of $2p$-$3s$ to $2p$-$3d$ resonance to resonance line ratios for Se XXV [Fig. 6(b)].

Se XXV and Se XXVI intraion ratios suggest most likely a consistent density using either Fig. 13(a) or 13(b). The low CRE density inferred from Fig. 13 might indicate that the plasma producing the spectrum was not in equilibrium. When electrons are heated faster than the ionization balance can follow, excitation rates are larger than in CRE because the exponential factors, $e^{-\Delta E/kT_e}$, in these rates are larger. However, because the $3d$ states have greater excitation energies, ΔE, than the $3s$ states, the excitation rate increases would be less for the $3d$ than for the $3s$ states. Thus $3s$ emission rates would increase faster than those of the $3d$ states, and the $2p$-$3s$ to $2p$-$3d$ ratio would increase as the degree of nonequilibrium increased.

Finally, there are plasmas for which the L-shell spectrum is dominated by neonlike lines. One example is provided by the spectrum of selenium shown by Burkhalter and Nagel [37] obtained from a laser-produced plasma. More recently a second example is provided by a bromine plasma produced by laser irradiation of a microdot. It was analyzed in Ref. [15] for independent determinations of an electron temperature and a charge-state distribution. The spectrum of Ref. [37] shows the Se XXV $n=2$-3 lines and all the satellites to these lines, but does not show any Se XXVI lines. Since the satellite lines to the Ne-like resonance lines are distinct and isolated, an analysis (similar to the analysis carried out with the spectrum in Ref. [47]) of ratios of temperature-sensitive satellites of $2p$-$3d$ lines to the parent resonance lines and density sensitive $2p$-$3s$ resonance to $2p$-$3d$ resonance lines within the neonlike Se XXV system can be used to infer simultaneously a temperature T_e and a density n_i of the plasma. The overlapping contours of these ratios that would be used to make these inferences are shown in Fig. 14.

IV. SUMMARY

The use of a line or line cluster ratio to infer either the temperature or the density of a plasma is limited, since these ratios can be dependent, in general, on both temperature and density. By displaying these dependences on two or more contour plots, one can make a more self-consistent determination of the plasma electron temperature jointly with the ion density provided the contour plots accurately represent these dependences. In turn, the accuracy of the line ratio contours

depends on the self-consistency and accuracy of the underlying atomic model and the ionization calculations. In the calculations of this paper, the populations of all ground as well as all singly excited states were obtained self-consistently in CRE by solving a single set of rate equations. These solutions included the non-LTE distribution of populations for each multiplet of $n=3$ states in both neonlike and fluorinelike ions.

The DBEX level populations that are needed for the satellite line calculations, on the other hand, were obtained in coronal model approximation by post-processing the rate equation solutions. This processing was done under the assumption that the DBEX states are formed by dielectronic capture and by ISE from the two adjacent ion states; that is, collisional couplings among the DBEX states were neglected in the post-analysis. In a dense plasma, the collisional mixing of DBEX states significantly alters their populations. The neglect of these density effects, therefore, is a potential source of error in the satellite line emission calculations at high densities.

Analyses of experimental spectra using the contours presented in this paper have several limitations, and there was some suggestion of their presence in the example given in this paper: the analysis of the spectrum in Ref. [47]. In laboratory plasmas, x-ray emission is often a highly transient event. In a rapidly heated laser-produced or z-pinch plasma, for example, ionization and recombination times may be too long for the plasma to remain in equilibrium, so a CRE assumption may break down and time-dependent or transient equations would need to be solved to determine the ionization states. A rapid time variation of electron temperatures alters the strengths of recombination versus excitation and ionization, and has significant effects on the line ratios. Since ISE becomes more important with increasing temperature, its contribution to the intensity of satellite lines and hence on the variation of the dielectronic to resonance line ratios become more significant in transient calculations. It is also possible that intense heating will generate non-Maxwellian electron distributions, which are predicted to have non-negligible effects on the line ratios and hence on the diagnostics of these strongly heated plasmas [1,48–50].

Even when the ionization state of a transient plasma stays close to equilibrium, the plasma may contain temperature and density gradients that turn temperature and density inferences into average inferences at best. One measure of the size of these gradients can be provided by making several determinations of temperature and density using different combinations of satellite and resonance line ratios [13]. In this case, one has more than two spectral features to match in order to obtain two quantities: T_e and n_i. For fluorinelike and neonlike spectrum, for example, one might try to match both fluorine- and neonlike intraion $2p$-$3s$ to $2p$-$3d$ ratios as well as the fluorinelike to neonlike $2p$-$3d$ ratio. Line ratios can also be affected by opacity. When photoexcitations and photoionizations become comparable to collisional excitations and ionizations, rate equation solutions that neglect these photopumping processes no longer apply.

Finally, we note that in future high-current driven, z-pinch experiments, for example, involving medium to high-Z plasmas, rapid ''burn-through'' in the L shell is required to generate K-shell ions. This burn-through is inhibited by L-shell radiation losses [51], and it is doubtful, when calculating this effect, that a detailed level accounting can be simplified by an averaging process such as used in the average atom model, which will inhibit all the important and relevant atomic radiation dynamics. One will need to determine experimentally how long the plasma remains in the L shell, and how fast the plasma ionizes and burns through to the K-shell states. Data analyses utilizing line cluster ratio contour plots of the kind presented in this paper will be needed to carry out this determination.

ACKNOWLEDGMENTS

We would like to thank Dr. P. E. Pulsifer for the valuable computer-related assistance he has provided in helping us to document the results of this work. This work was supported by the Defense Special Weapons Agency and the Office of Naval Research.

[1] J. P. Matte, J. C. Keifer, S. Ethier, M. Chaker, and O. Peyrusse, Phys. Rev. Lett. **72**, 1208 (1994).
[2] M. C. Coulter, K. G. Whitney, and J. W. Thornhill, J. Quantum Spectrosc. Radiat. Transfer **44**, 443 (1990).
[3] V. A. Boiko, S. A. Pikuz, and A. Ya. Faenov, J. Phys. B **12**, 1889 (1979).
[4] A. Zigler, V. L. Jacobs, D. A. Newman, P. G. Burkhalter, D. J. Nagel, T. S. Nuk, A. McPherson, K. Boyer, and C. K. Rhodes, Phys. Rev. A **45**, 1569 (1992).
[5] A. K. Pradhan and J. M. Shull, Astrophys. J. **249**, 821 (1981).
[6] P. W. Vedder, C. R. Canizares, T. H. Markert, and A. K. Pradhan, Astrophys. J. **307**, 269 (1986).
[7] J. Green, P. Jelinsky, and S. Bower, Astrophys. J. **359**, 499 (1990).
[8] F. P. Keenan, K. H. J. Philips, L. K. Harra, E. S. Conlon, and A. E. Kingston, Astrophys. J. **393**, 815 (1992).
[9] M. Bitter *et al.*, Phys. Rev. Lett. **71**, 1007 (1993).
[10] K. D. Zastrow, E. Kalline, and H. P. Summers, Phys. Rev. A **41**, 1427 (1990).
[11] J. D. Kilkenny, R. W. Lee, M. H. Key, and J. G. Lunney, Phys. Rev. A **22**, 2746 (1980).
[12] B. Yaakobi *et al.*, Phys. Rev. A **19**, 1247 (1979).
[13] J. P. Apruzese, K. G. Whitney, J. Davis, and P. C. Kepple, J. Quantum Spectrosc. Radiat. Transfer **57**, 41 (1997).
[14] C. J. Keane, B. A. Hammel, A. L. Osterheld, and D. R. Kania, Phys. Rev. Lett. **72**, 3029 (1994).
[15] W. H. Goldstein, R. S. Walling, J. Bailey, M. H. Chen, R. Fortner, M. Klapisch, T. Phillips, and R. E. Stewart, Phys. Rev. Lett. **58**, 2300 (1987).
[16] S. Ya. Khakhalin, B. A. Bryunetkin, I. YU. Skobelev, A. Ya. Faenov, J. Nilsen, A. L. Osterheld, and S. A. Pikuz, Zh. Éksp. Teor. Fiz. **105**, 118 (1994) [Sov. Phys. JETP **78**, 633 (1994)].
[17] J. Bailey, R. E. Stewart, J. D. Kilkenny, R. S. Walling, T. Phillips, R. J. Fortner, and R. W. Lee, J. Phys. B **19**, 2639 (1986).

[18] D. A. Liedahl, S. M. Kahn, A. L. Osterheld, and W. H. Goldstein, in *High Resolution X-Ray Spectroscopy of Cosmic Plasmas*, edited by P. Georenstein and M. Zombeck (Cambridge University Press, Cambridge, 1990), IAU Colloq. No. 115, p. 49.
[19] A. H. Gabriel, Mon. Not. R. Astron. Soc. **160**, 99 (1972).
[20] A. H. Gabriel and T. M. Paget, J. Phys. B **5**, 673 (1972).
[21] A. Dasgupta, K. G. Whitney, M. Blaha, and M. Buie, Phys. Rev. A **46**, 5973 (1992).
[22] D. H. Sampson, H. L. Zhang, A. K. Mohanty, and R. E. H. Clark, Phys. Rev. A **40**, 604 (1989).
[23] H. L. Zhang, D. H. Sampson, and A. K. Mohanty, Phys. Rev. A **40**, 616 (1989).
[24] D. H. Sampson, H. L. Zhang, and C. J. Fontes, At. Data Nucl. Data Tables **48**, 25 (1991).
[25] H. L. Zhang and D. H. Sampson, Phys. Rev. A **47**, 208 (1993).
[26] H. L. Zhang and D. H. Sampson, Phys. Rev. A **42**, 5378 (1990).
[27] H. L. Zhang and D. H. Sampson, Atom. Data Nucl. Data Tables **43**, 1 (1989).
[28] D. H. Sampson and H. L. Zhang, Phys. Rev. A **45**, 1657 (1992).
[29] Atomic structure code of R. D. Cowan following his book *The Theory of Atomic Structure and Spectra* (University of California Press, Berkeley, CA, 1981).
[30] J. Abdallah, Jr., R. E. H. Clark, and R. D. Cowan (unpublished).
[31] R. E. H. Clark, J. Abdallah, Jr., G. Csanak, J. B. Mann, and R. D. Cowan (unpublished).
[32] P. Hagelstein and R. K. Jung, At. Data Nucl. Data Tables **37**, 121 (1987).
[33] K. G. Whitney and M. C. Coulter, IEEE Trans. Plasma Sci. **16**, 552 (1988).
[34] J. C. Raymond and B. W. Smith, Astrophys. J. **306**, 762 (1986).
[35] E. V. Aglitskiy, V. A. Boiko, O. N. Krokhin *et al.*, Kvant. Elektron. (Moscow) **1**, 2067 (1974) [Sov. J. Quantum Electron. **4**, 1152 (1975)].
[36] V. A. Boiko, A. Ya. Faenov, and S. A. Pikuz, J. Quantum Spectrosc. Radiat. Transfer **19**, 11 (1978).
[37] P. G. Burkhalter and D. J. Nagel, Phys. Rev. A **11**, 782 (1975).
[38] J. F. Seely *et al.*, Phys. Rev. A **34**, 2942 (1986).
[39] H. L. Zhang, D. H. Sampson, R. H. Clark, and J. B Mann, At. Data Nucl. Data Tables **37**, 17 (1987).
[40] R. D. Cowan, J. Phys. B **13**, 1471 (1980).
[41] L. B. Golden, D. H. Sampson, and K. Omidvar, J. Phys. B **11**, 3235 (1978).
[42] D. L. Moores, L. B. Golden, and D. H. Sampson, J. Phys. B **13**, 385 (1980).
[43] A. Dasgupta and K. G. Whitney, Phys. Rev. A **42**, 2640 (1990).
[44] A. Dasgupta and K. G. Whitney, At. Data Nucl. Data Tables **58**, 77 (1994).
[45] J. G. Lunney, Phys. Rev. A **40**, 467 (1989).
[46] V. L. Jacobs and M. Blaha, Phys. Rev. A **21**, 525 (1980).
[47] M. D. Rosen, P. L. Hagelstein, D. L. Matthews, E. M. Campbell, A. U. Hazi, B. L. Whitten. B. MacGowan, R. E. Turner, and R. W. Lee, Phys. Rev. Lett. **54**, 106 (1985).
[48] R. Bartiromo, F. Bombarda, and R. Giannella, Phys. Rev. A **32**, 531 (1985).
[49] A. H. Gabriel and K. J. H. Phillips, Mon. Not. R. Astron. Soc. **189**, 319 (1979).
[50] A. Dasgupta, K. G. Whitney, and P. E. Pulsifer, Bull. Am. Phys. Soc. **39**, 1205 (1994).
[51] J. Davis, J. L. Giuliani, Jr., and M. Mulbrandon, Phys. Plasmas **2**, 1766 (1995).